Journal of Luminescence 179 (2016) 402–407

Contents lists available at ScienceDirect

Journal of Luminescence

journal homepage: www.elsevier.com/locate/jlumin

Full Length Article

Detailed luminescence properties and laser potential of Pr:FAP

B. Qu [a,b,1], J.L. Doualan [a], B. Xu [b], A. Braud [a], Z.P. Cai [b], P. Camy [a], R. Moncorgé [a,*]

[a] Centre de Recherche sur les Ions, les Matériaux et la Photonique (CIMAP), UMR 6252CEA-CNRS-ENSICaen, Université de Caen, 6 Bvd. Maréchal Juin, 14050 Caen, France

[b] Department of Electronic Engineering, Xiamen University, Xiamen, Fujian 361005, China

ARTICLE INFO

Article history:
Received 7 November 2015
Received in revised form
25 July 2016
Accepted 26 July 2016
Available online 29 July 2016

Keywords:
Praseodymium
Fluoro-apatite
Near-infrared emission

ABSTRACT

Polarized absorption spectra are recorded from 400 nm to 2400 nm and analyzed within the framework of the Judd–Ofelt formalism. The best fit to the data is obtained by using the so-called "standard method" but by omitting the $^3H_4 \rightarrow {}^3P_2$ hypersensitive absorption transition from the fitting procedure. Polarized and continuous-wave as well as time-resolved emission spectra are registered for the first time between 450 nm and 1200 nm. Fluorescence lifetime measurements are performed at different emission and for different excitation wavelengths. The analysis of the data confirms the low emission quantum efficiency of the ($^3P_{0,1}$,$^1I_6$) set of thermalized emitting levels and the predominance of the emissions coming from the $^1D_2$ multiplet. It reveals the existence of an interesting near-infrared emission band coming from a $^1D_2 \rightarrow {}^3F_3$,$^3F_4$ emission transition and extending from about 1000 nm to 1150 nm with a peak emission cross-section of 6.2×10^{-20} cm^2 at 1073 nm.

1. Introduction

Efficient diode-pumped laser operation at many laser wavelengths across the visible spectral range has been recently demonstrated by using Pr-doped fluoride bulk crystals and glass fibers [1–18] and, to a lesser extent, because of larger phonon energies and increased inter-Stark levels non-radiative relaxations, by using some Pr-doped oxides [19–22].

It was also recently claimed that $Ca_5(PO_4)_3F$(also known as FAP), a fluoro-apatite crystal which was extensively studied with rare-earth dopants like Yb^{3+}because of very specific spectroscopic properties such as high and strongly polarized emission cross-sections, had favorable spectroscopic properties as a laser gain medium when it is doped with Pr^{3+} ions for the visible laser application [23]. This assertion was based on an older result [24] according to which the quantum efficiency of the usual $^3P_0$ emitting level for visible radiations was of the order of 98%.However, according to the pioneer's work of L.D. Merkle et. al [25,26] such assertion may be incorrect. Indeed, first, there is an obvious confusion in the literature about the concentration of Pr^{3+}in reference [24], since it is stated that it represents $4.51 \times 10^{20} Pr^{3+}$ ions/cm^3 for a 1 wt% doped Pr:FAP sample, while such dopant concentration actually means 1.37×10^{20} ions/cm^3. Consequently, the Judd–Ofelt analysis which is subsequently performed in this article and the derived laser parameters, including the above mentioned quantum efficiency, certainly need to be re-examined. Moreover, considering that the segregation coefficient of Pr^{3+} in FAP is only 0.89 [26], the real concentration should be about 1.2×10^{20} ions/cm^3. This value is very close to the value given in [25] where there is also some confusion since this value is given for a nominal concentration of 1at% instead of 1 wt%. Finally, according to L.D. Merkle et al. [25], by room temperature, the emission should be dominated by a $^1D_2$ emission regardless of the excitation wavelength. The emission lifetime of the $^3P_0$ level would be of the order of hundreds of ns [26], thus less than 1 μs (not 75 μs as reported in [23]), and that for $^1D_2$ of the order of 65 μs for sites A [26]. In that hypothesis, the emission quantum efficiency of the $^3P_0$ level would be fairly small.

Therefore, our purpose here in this communication is to present a more complete luminescence study of Pr:FAP than was reported in the past and to really determine the emission characteristics and the laser potential of this material in the visible but also in the near-infrared emission domain around 900 nm. Indeed, a very interesting broadband emission was evidenced in past in this rarely explored spectral range in Pr-doped ZBLAN [27], another fluoro-oxide, and efficient and tunable CW laser operation could be very recently demonstrated between about 860 and 930 nm, thus over 70 nm, in the case of Pr:YLF [28].

Section 2 is devoted to the crystallographic and optical properties of Pr:FAP. Section 3 is dedicated to a presentation and a

* Corresponding author.
E-mail address: richard.moncorge@ensicaen.fr (R. Moncorgé).
[1] Present address: Department of Electronic Engineering, Xiamen University, Xiamen, Fujian 361005, China.

http://dx.doi.org/10.1016/j.jlumin.2016.07.048
0022-2313/

Judd–Ofelt analysis of the polarized absorption spectra registered at room temperature between 400 and 2500 nm. Section 4 reports polarized continuous-wave and time-resolved emission spectra along with fluorescence decays registered at room temperature under selective laser excitation. Section 5 is dedicated to a discussion of the results and Section 6 to the conclusions which can be derived.

2. Crystal properties

$Ca_5(PO_4)_3F$ (or FAP) crystallizes with the hexagonal space group $P6_3/m$. There are two formula units in each unit cell and the Ca^{2+} ions occupy two types of nonequivalent sites labeled M_1 or Ca II (4f sites) with C_3 symmetry, and M_2 or Ca I (6h sites) with C_s symmetry [29,30]. Trivalent rare-earth dopants like Pr^{3+} substitute for these Ca^{2+} cations with, according to [26], occupation ratios of about 40% and 60%, respectively. Consequently, the spectroscopic properties of Pr:FAP should reflect the uniaxial nature of the host matrix and the two different types of lattice environments and local crystal-fields experienced by the Pr^{3+} active ions.

The refractive indices for the *a*- and *c*-axis directions which will be necessary in the forthcoming Judd–Ofelt analysis are given by the following Sellmeier relations:

$$n_a^2 = 2.626769 + \frac{0.014626}{\lambda^2 - 0.012833} - 0.007653\lambda^2 \quad (1)$$

$$n_c^2 = 2.620175 + \frac{0.014703}{\lambda^2 - 0.011037} - 0.007544\lambda^2 \quad (2)$$

The sample used for our measurements was a 1.0 wt% Pr^{3+}-doped crystal which means, considering the segregation coefficient of 89% indicated in [26], an actual dopant concentration 0.89 wt% Pr^{3+} corresponding to about 1.18×10^{20} Pr^{3+} ions/cm^3.

3. Polarized absorption spectra and Judd–Ofelt analysis

Only unpolarized absorption spectra were reported in the past literature [24,25]. Absorption spectra reported here in Fig. 1 were registered at room temperature both in π ($E//c$) and σ ($E/\perp c$) polarizations from 400 nm to 2400 nm. The spectra were registered with a Perkin-Elmer Lambda 1050 spectrophotometer. The *c* axis of the crystal was perpendicular to the optical axis and the polarized spectra were registered with adequate polarizers.

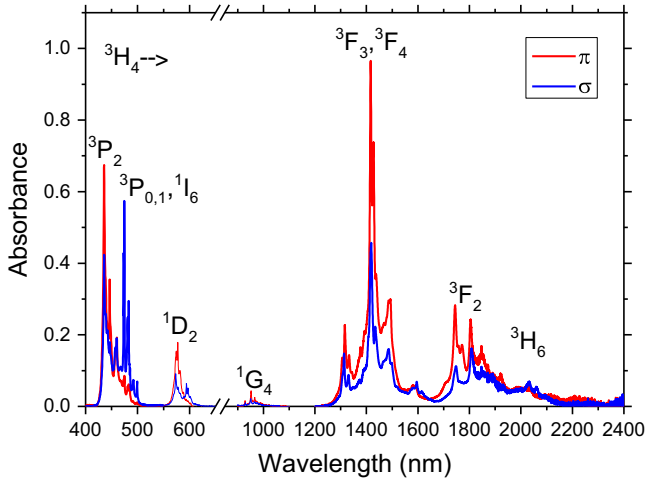

Fig. 1. Room temperature polarized absorption spectra of Pr:FAP.

The various peaks observed in these spectra are easily assigned to the usual ff inter-multiplet absorption transitions which characterize the Pr^{3+} ion in this wavelength domain. As it is often the case, because of many overlapping components, it is difficult to discriminate between the transitions from the $^3H_4$ ground-state to the $^3P_0$, $^3P_1$ and $^1I_6$, and to the $^3F_3$ and $^3F_4$ multiplets. This is the reason why these two sets of optical transitions will be treated without any deconvolution in the following Judd–Ofelt analysis.

It is noticed first that several absorption lines, around 450 nm and 570 nm more specifically, which correspond to the spin-allowed and spin-forbidden $^3H_4 \rightarrow {}^3P_{0,1,2}, {}^1I_6$ and $^3H_4 \rightarrow {}^1D_2$ absorption transitions, respectively, are strongly polarized. It is also noticed the complex structure of each of these transitions which likely results from the multisite nature of the Pr^{3+} ions in this particular material and which was already discussed in [26].

Although a Judd–Ofelt treatment does not really make sense in the case of a multisite system for which it is illusory, especially at room temperature, to discriminate between the transitions coming from the different sites, it will be performed here however to compare the results with those reported in [24] and [25] where we noticed some confusions concerning the actual dopant concentration and the Judd–Ofelt procedure.

The Judd–Ofelt analysis was performed by using so-called standard, normalized and modified methods, as in [24]. However, in contrast with [25], we discarded the intense hypersensitive absorption transition to the $^3P_2$ multiplet around 437 nm from the fitting procedure to avoid the derivation of an unrealistic negative Ω_2 parameter, as it is made for instance in [31].

The standard method, as introduced by Judd and Ofelt [32,33], consists in calculating first electric-dipole transition strengths $S^{ed}_{meas}(J \rightarrow J')$ according to the expression:

$$S^{ed}_{meas}(J \rightarrow J') = \frac{9n}{(n^2+2)^2}\left[\frac{3ch\varepsilon_0(2J+1)}{2\pi^2\bar{\lambda}e^2}\left(\int \sigma_{abs}(\lambda)d\lambda\right) - n.S^{md}_{calc}(J \rightarrow J')\right] \quad (3)$$

where J and J' are the total angular momentum quantum numbers of the initial and final states, c is the light velocity, h is the Planck constant, e is the free electron charge, n is the refractive index obtained from Eqs. (1) and (2) by writing $n(\lambda) = \frac{1}{3}[n_c(\lambda) + 2n_a(\lambda)]$, $\bar{\lambda}$ is the average wavelength and $\sigma_{abs}(\lambda) = \frac{1}{3}[\sigma^{\pi}_{abs}(\lambda) + 2\sigma^{\sigma}_{abs}(\lambda)]$ the measured absorption cross section of the concerned transition averaged over both polarizations. $S^{md}_{calc}(J \rightarrow J')$ is a magnetic dipole line strength contribution which can be calculated by using the following expression [34]:

$$S^{md}_{calc}(J \rightarrow J') = \left| < (S,L)J \,||\, L + 2S \,||\, (S',L')J' > \right|^2 \quad (4)$$

where $|(S,L)J>$ and $|(S',L')J'>$ are the initial and final transition states, and $<||L+2S||>$ are the matrix elements for the magnetic dipole transitions.

Then, a least square fit of (3) is performed with the theoretical expression

$$S^{ed}_{calc}(J \rightarrow J') = \sum_{t=2,4,6} \Omega_t \left| < (S,L)J \,||\, U^{(t)} \,||\, (S',L')J' > \right|^2 \quad (5)$$

where the $<||U^{(t)}||>$ stand for tabulated matrix elements [35] and Ω_2, Ω_4 and Ω_6 are adjustable "intensity" parameters. In this case, the quality of the fitting is estimated by calculating the root mean square (RMS) deviation defined by the expression:

$$RMS = \sqrt{\frac{\sum_{i=1}^{q}\left(S^{ed}_{meas} - S^{ed}_{calc}\right)^2}{q-p}} \quad (6)$$

where q is the number of chosen transitions and $p=3$ the number of derived intensity parameters. Here $q=6$ since fittings of experimental data were performed by calculating in Exp. (3) the

Please cite this article as: B. Qu, et al., J. Lumin. (2016), http://dx.doi.org/10.1016/j.jlumin.2016.07.048

integrated absorption cross sections $\int \sigma_{abs}(\lambda)d\lambda$ for the absorption transitions to the 6 sets of excited multiplets (see in Fig. 1) : ($^3P_{0,1}$,$^1I_6$), $^1D_2$, $^1G_4$, ($^3F_3$,$^3F_4$), $^3F_2$ and $^3H_6$ around 450 nm, 580 nm, 950 nm, 1450 nm, 1800 nm and 2050 nm, respectively.

In the normalized method, the fitting of the intensity parameters is determined by:

$$\frac{\sum_{t=2,4,6} \Omega_t |<(S,L)J||U^{(t)}||(S',L')J'>|^2}{S^{ed}_{calc}(J\rightarrow J')} = k \quad (7)$$

where k is a coefficient which is often set as one. This method is often preconized to more properly account of the weak transitions [36,37]. In the fitting procedure, the corresponding normalized (or relative) *RMS* deviation to be minimized is given by:

$$RMS = \sqrt{\frac{\sum_{i=1}^{q}\left(\frac{S^{ed}_{meas}-S^{ed}_{calc}}{S^{ed}_{meas}}\right)^2}{q-p}} \quad (8)$$

where q and p are the same as defined above.

In the modified method, a correction is introduced to account for the influence of the $4f^{n-1}5d$ excited-state electronic configuration. The modified electric dipole line-strength then is expressed by inserting an energy dependent factor as follows [36,38]

$$S^{ed}_{calc}(J\rightarrow J') = \sum_{t=2,4,6} \Omega_t \left[1+2\alpha(E(J)+E(J') - 2E(4f))\right] |<(S,L)J||U^{(t)}||(S',L')J'>|^2 \quad (9)$$

where $E(J)$ and $E(J')$ are the energy of the initial and final states of the concerned transition, $E(4f)=9940\ cm^{-1}$ is the mean energy of the $4f^n$ electronic configuration and $\alpha = 1/[2(E(4f5d)-E(4f))] \approx 1.66\times10^{-5}$ cm in the case of Pr:FAP, as derived in [25]. The RMS deviation between measured and calculated line strengths is given by the same expression (8) as for the normalized method.

The best fits were obtained with the standard and the normalized methods with RMS values of $0.65\times10^{-20}\ cm^2$ and $0.51\times10^{-20}\ cm^2$, respectively. However, the normalized method gives a better agreement for the absorption transition to the $^3H_6$ than to the ($^3F_3$, $^3F_4$) multiplets while the standard method does the reverse. On the other hand, as shown in Fig. 1, the band corresponding to the absorption transition to the $^3H_6$ multiplet is much weaker than the other and its deconvolution from the band corresponding to the absorption transition to the $^3F_2$ multiplet is not very precise. Consequently, choice was made for the results given by the standard method for which it is obtained the Judd–Ofelt intensity parameters:

$\Omega_2 = 0.76\times10^{-20}\ cm^2$, $\Omega_4 = 10\times10^{-20} cm^2$ and $\Omega_6 = 6.42\times10^{-20}\ cm^2$

Using these parameters, it is also derived the radiative lifetimes and branching ratios reported in the Table 1.

Table 1
Radiative lifetimes and branching ratios of the main emission transitions from levels $^3P_0$ and $^1D_2$.

Upper manifold states and lifetime	Branching ratio (%)		Upper manifold states and lifetime	Branching ratio (%)	
	$^1G_4$	6.6		$^1G_4$	2.2
	$^3F_{3,4}$	10.6		$^3F_{3,4}$	13.6
$^1D_2\rightarrow$	$^3F_2$	19.6	$^3P_0\rightarrow$	$^3F_2$	3.4
293 μs	$^3H_6$	21	15 μs	$^3H_6$	8.7
	$^3H_5$	1		$^3H_5$	0
	$^3H_4$	41		$^3H_4$	71.8

It is also found the radiative lifetimes τ_R ($^1I_6$)=74 μs and τ_R ($^3P_1$)=16 μs.

This markedly differs from the results reported in [25] where the best fit to the absorption data was obtained by using the modified method and for the intensity parameters $\Omega_2 = -8.6\times10^{-21}\ cm^2$, $\Omega_4 = 4.9\times10^{-20}\ cm^2$ and $\Omega_6 = 1.9\times10^{-20}\ cm^2$, which gives in turn the radiative lifetimes τ_R ($^3P_0$)=71 μs and τ_R ($^1D_2$)=1 ms (although in [25] there is probably a typing error since it is also written τ_R ($^3P_0$)=1 ms).

4. Polarized and time-resolved emission spectra

Continuous-wave (CW) and time-resolved emission spectra as well as fluorescence decays were registered by exciting the sample at 435 nm, 445 nm and 571 nm, therefore in the $^3P_2$, ($^3P_{0,1}$,$^1I_6$) and $^1D_2$ multiplets, respectively.

We show in the Fig. 2 the polarized emission spectra which were obtained between 450 nm and 1200 nm by pumping the crystal around 445 nm with a CW InGaN laser diode. These spectra were corrected for the spectral response of the apparatuses (a standard 1200 grooves/mm HRS2 Jobin-Yvon monochromator and a R5108 Hamamatsu photomultiplier). Comparing these spectra with those obtained for instance for Pr:YLF, for which emission transitions in this visible to near-infrared wavelength domain mainly occur from the thermalized set of energy levels $^3P_0$, $^3P_1$ and $^1I_6$ [28,39], and for Pr:PANK, a Pr-doped phosphate glass for which emission transitions originate both from the $^3P_0$ and $^1D_2$ multiplet [40], it is clear that the emission spectra for Pr:FAP more closely resemble to the latter than the former. This means that if the emission peaks found around 500 nm can be undoubtedly assigned to ($^3P_{0,1}$,$^1I_6$)→$^3H_4$ emission transitions, those found between 580 nm and 1150 nm must be coming from both ($^3P_{0,1}$,$^1I_6$) and $^1D_2$ emitting multiplets down to lower lying ones. Between about 580 nm and 660 nm, there should be a juxtaposition of transitions from the ($^3P_{0,1}$,$^1I_6$) to the $^3H_6$ and $^3F_2$ levels with transitions from the $^1D_2$ down to the $^3H_4$ level. Between 660 nm and 750 nm, there should a juxtaposition of ($^3P_{0,1}$,$^1I_6$)→$^3F_3$,$^3F_4$ and $^1D_2$→$^3H_5$ emission transitions. Between 820 nm and 925 nm, it could be a juxtaposition of ($^3P_{0,1}$,$^1I_6$)→$^1G_4$ (as it was recently demonstrated in the case of Pr:$LiYF_4$[28]) and $^1D_2$→$^3H_6$ and $^3F_2$ transitions. On the other hand, however, the broad and intense emission band which appears between about 980 nm and 1150 nm, an emission feature which is observed and reported here for the first time, can be only assigned to $^1D_2$→$^3F_3$,

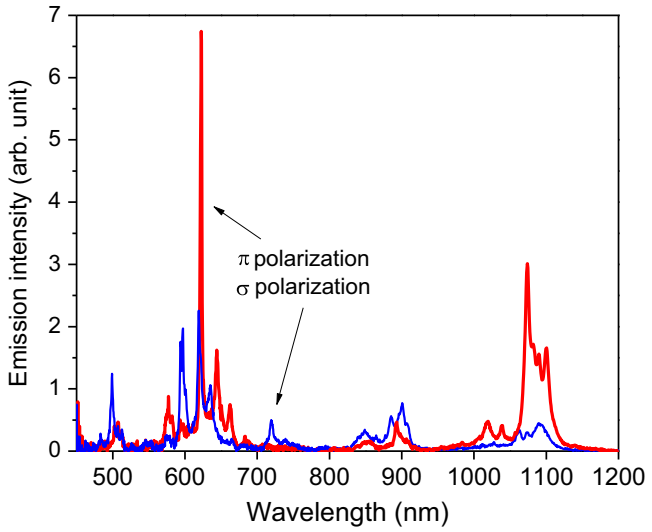

Fig. 2. Continuous-wave polarized emission spectra.

Please cite this article as: B. Qu, et al., J. Lumin. (2016), http://dx.doi.org/10.1016/j.jlumin.2016.07.048

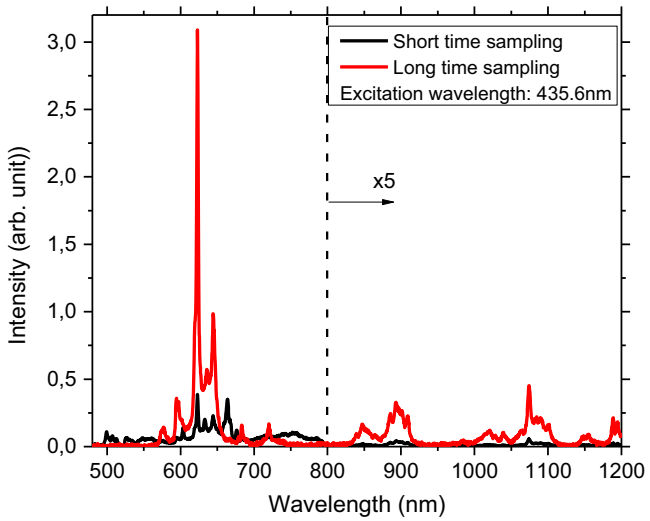

Fig. 3. Time-resolved emission spectra obtained at short- and long-time delays (between 380 ns and 1.58 μs, and between 10 and 40 μs, respectively) after pulsed laser excitation at 435.6 nm.

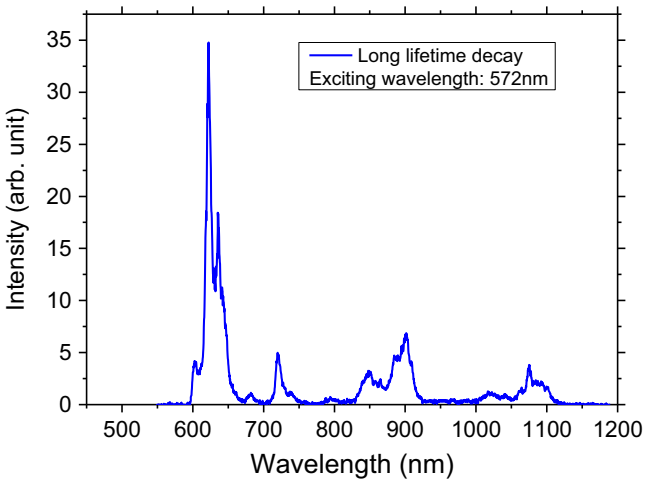

Fig. 4. Time-resolved emission spectrum obtained at long-time delay (between 10 and 40 μs) after pulsed laser excitation at 572 nm.

$^3F_4$ transitions. The comparison of the Pr:FAP spectra with those of Pr:YLF and Pr:PANK also indicates that emissions coming from the $^1D_2$ multiplet should dominate, which indicates in turn, in agreement with the conclusions of [25] but in contradiction with those of [23] and [24], that a strong non-radiative multiphonon relaxation occurs between levels ($^3P_{0,1}$,$^1I_6$) and $^1D_2$.

Such a non-radiative relaxation was first confirmed by recording the fluorescence lifetimes of the 500 nm emission which is found equal to about 260 ns, thus again in close agreement with the value of about 150 ns reported in [25,26] against a value of 78 μs in the case of [24]. Fluorescence decay measurements were also performed at different wavelengths across the emission spectra. It results in more or less non-exponential decays with dominant long-time components associated with fluorescence time constants ranging between 35 and 50 μs, in good agreement with the value of 35 μs reported in [25,26], such non-exponential decays being attributed to the complex multisite structure and the different lattice sites occupied by the Pr^{3+} ions in Pr:FAP.

The dominant contribution of the $^1D_2$ emissions and the complex structure of the emission spectra were further checked by exciting the sample at 435.6 nm, thus again in the $^3P_2$ absorption band, but also at 572 nm, thus directly into the $^1D_2$. For that purpose, use was made of the tunable pulsed radiation (6 ns laser pulses) of a standard OPO (Optical Parametric Oscillator) and the emission spectra were registered at different time delays after the exciting laser pulse.

Fig. 3 shows for instance the emission spectra which are obtained by exciting the crystal at 435.6 nm and by recording the emission intensity between 380 ns and 1.58 μs (short time sampling) then between 10 and 40 μs (long time sampling) after the laser pulse. It is clear that the long-time spectrum is much more intense that the one recorded at short time. Since the emission transitions coming from the ($^3P_{0,1}$,$^1I_6$) levels should be very short lived emission transitions, the peaks which appear at short time delay can be predominantly assigned to these emitting levels. This is the case of the peaks which appear between 600 nm and 665 nm and of the band peaking around 750 nm. On the other hand, the spectrum which is registered at long-time delay is predominantly attributed to the $^1D_2$ emitting level, with peaks between 570 nm and 750 nm, between 830 nm and 920 nm, and between 1000 nm and 1120 nm. The peaks which appear in the spectrum between 1150 nm and 1200 nm do not correspond to any emission transitions. They are second order replicas of the peaks which occur between 570 nm and 600 nm.

In the end, Fig. 4 shows the spectrum which is obtained by exciting the sample at 572 nm, thus directly into the $^1D_2$ level, and by sampling the signal at long-time delay, thus again between 10 and 40 μs after the excitation laser pulse, and knowing that the same result is obtained at short times. This spectrum is similar between 680 and 1100 nm to that obtained by exciting at 435.6 nm and by sampling the signal at long-time delay. It clearly reproduces the main emission features lying around 720 nm, 870 and 1050 nm. However, these spectra are not quite consistent between each other around 620 nm. The intensity ratio of the lines observed for instance around 900 and 622 nm strongly differ. This is to be attributed to some up-conversion energy transfer process taking place in the directly excited $^1D_2$ level that populates the ^3P_J manifold, something already noticed in the past in the case of Pr:LaF_3[41,42] and Pr:FAP [26]. Due to the long emission lifetime of the $^1D_2$ excited level, such an up-conversion process indeed introduces a long time component in the resulting ^3P_J fluorescence decay and when time-resolved emission spectra are recorded at long-time delays in such conditions, both $^1D_2$ and ^3P_j emissions can be observed. This is clearly what happens around 620 nm where both energy levels can contribute.

5. Discussion of the results

The branching ratios which could be derived from the Judd–Ofelt analysis of the absorption spectra can be confronted first with those which can be calculated from the calibrated emission spectra reported in Fig. 2 and by assuming that these spectra predominantly come from the $^1D_2$ emitting level. According to the Judd–Ofelt analysis (see in Table 1), the branching ratios β_1 and β_2 corresponding to the $^1D_2 \rightarrow {}^3H_{4,5}$ and $^1D_2 \rightarrow {}^3H_6,{}^3F_{2,3,4}$ emission transitions occurring between 570 and 750 nm and between 800 and 1150 nm, respectively, are found equal to:

$\beta_1 \approx 0.42$ and $\beta_2 \approx 0.51$

Those which can be estimated experimentally from the emission spectra are found equal to

$$\beta_1 = \frac{\int_{570-750\ \mathrm{nm}} \lambda[I^{\pi}(\lambda)+2I^{\sigma}(\lambda)]}{\int_{570-1150\ \mathrm{nm}} \lambda[I^{\pi}(\lambda)+2I^{\sigma}(\lambda)]} \approx 0.38 \text{ and}$$

$$\beta_2 = \frac{\int_{800-1150\ \mathrm{nm}} \lambda[I^{\pi}(\lambda)+2I^{\sigma}(\lambda)]}{\int_{570-1150\ \mathrm{nm}} \lambda[I^{\pi}(\lambda)+2I^{\sigma}(\lambda)]} \approx 0.62$$

Please cite this article as: B. Qu, et al., J. Lumin. (2016), http://dx.doi.org/10.1016/j.jlumin.2016.07.048

In view of the uncertainties inherent to any Judd-Ofelt analysis and of the method used to experimentally estimate these branching ratios by neglecting the emissions from the ($^3P_{0,1}$,$^1I_6$) levels and the infrared ones coming from both ($^3P_{0,1}$,$^1I_6$) and $^1D_2$ levels and lying beyond 1200 nm, the agreement between calculated and measured branching ratios is rather satisfactory, thus giving more credit to the above Judd–Ofelt analysis and results.

The measured fluorescence lifetimes can be confronted in turn with the radiative lifetimes derived from the Judd–Ofelt analysis to give a rough estimation of the emission quantum efficiencies of the $^3P_0$ and $^1D_2$ emitting levels. With a fluorescence lifetime $\tau_F \approx$ 260 ns for a radiative one $\tau_R \approx$ 15 μs, the emission quantum efficiency $\eta = \tau_F/\tau_R$ for the $^3P_0$ emitting level should not exceed 1.7%. This is far smaller than the value of 98% reported in [23,24]. Such a low quantum efficiency likely comes from the large phonon energies which characterize calcium fluoro-apatite $Ca_5(PO_4)_3F$, up to about 3600 cm^{-1}[43] compared to 495 cm^{-1} in the case of $LiYF_4$. For the same reason, the emission quantum efficiency of level $^1D_2$ is also relatively reduced. Indeed, with a fluorescence lifetime not exceeding about 50 μs for a radiative one of about 293 μs, we end with a quantum efficiency η ($^1D_2$) $\leq$ 17%. In the end, by assuming again that the emission bands reported in Fig. 2 beyond 550 nm can be not exclusively but predominantly assigned to $^1D_2$ emission transitions (like in the case of the Pr:PANK glass, see in the Fig. 2(a) of [40]), it is possible to give a rough estimate of the emission cross sections of the various emission peaks around 622 nm, 901 nm and 1073 nm by using the well-known Fuchtbauer-Ladenburg expression:

$$\sigma_{em}(\lambda) = \frac{3\lambda^5}{8\pi n^2 c \tau_R} \frac{I(\lambda)}{\int \lambda [I^{\pi}(\lambda) + 2I^{\sigma}(\lambda)]} \quad (10)$$

With τ_R ($^1D_2$)=293 μs (see in Table 1), it is found the cross-sections values σ^{π}_{em} (622 nm)=9.1×10^{-21} cm^2, σ^{σ}_{em} (901 nm)=6.4×10^{-21} cm^2 and σ^{π}_{em} (1073 nm)=6.2×10^{-20} cm^2, thus rather large emission cross sections, especially in the case of the 1073 nm emission peak.

6. Conclusion

Polarized absorption spectra registered at room temperature from 400 to 2400 nm have been analyzed within the framework of the Judd–Ofelt formalism and a good fit between experimental and calculated transition cross sections has been obtained by using the so-called standard method.

Emission spectra have been registered by exciting the sample at different excitation wavelengths either continuously or with a pulsed laser and at short- and long-time delays after the exciting laser pulse, from 500 to 1200 nm. Fluorescence decays were also recorded for different excitation and emission wavelengths.

Confrontation of the radiative emission lifetimes derived from the Judd–Ofelt analysis of the absorption spectra with the various fluorescence time-constants derived from the measured fluorescence decays show that at room temperature the $^1D_2$ emissions predominate over that coming from the thermalized ($^3P_{0,1}$,$^1I_6$) levels for any excitation wavelengths because of strong non-radiative multiphonon relaxations due to particular large phonon energies. It corroborates and reinforced the conclusions reached in [25,26], but it contradicts those presented in [23,24] and according to which levels ($^3P_{0,1}$,$^1I_6$) could emit with a emission quantum efficiency close to about 98%.

Use has been made of the above derived radiative lifetimes and of the calibrated emission spectra to estimate the emission cross section of the various emission transitions. A value of 6.2×10^{-20} cm^2 is obtained for the peak at 1073 nm of a broad band emission reported here for the first time and lying between about 1000 and 1150 nm and attributed to $^1D_2 \rightarrow {}^3F_3$,$^3F_4$ emission transitions, showing the possibility of achieving laser operation in this interesting wavelength domain with a reduced but non-negligible efficiency.

Acknowledgments

Part of this work has been performed within the framework of the CSC (China Scholarship Council) grant 342 of one of us (B.Q) and a more extensive collaboration on Pr-doped laser materials with the Department of Electronic Engineering of Xiamen University.

References

[1] T. Gün, P. Metz, G. Huber, Opt. Lett. 36 (6) (2011) 1002.
[2] B. Xu, P. Camy, J.L. Doualan, Z. Cai, R. Moncorgé, Opt. Express 19 (2) (2011) 1191.
[3] P.W. Metz, F. Reichert, F. Moglia, S. Müller, D.T. Marzahl, C. Kränkel, G. Huber, Opt. Lett. 39 (11) (2014) 3193.
[4] W. Bolanos, G. Brasse, F. Starecki, A. Braud, J.L. Doualan, R. Moncorgé, P. Camy, Opt. Lett. 39 (15) (2014) 4450.
[5] Z. Liu, Z.P. Cai, S.L. Huang, C.H. Zeng, Z.Y. Meng, Y.K. Bu, Z.Q. Luo, B. Xu, H.Y. Xu, C.C. Ye, F. Stareki, P. Camy, R. Moncorgé, J. Opt. Soc. Am. B 30 (2) (2013) 302.
[6] F. Cornacchia, A. Richter, E. Heumann, G. Huber, D. Parisi, M. Tonelli, Opt. Express 15 (3) (2007) 992.
[7] D. Paboeuf, O. Mhibik, F. Bretenaker, P. Goldner, D. Parisi, M. Tonelli, Opt. Lett. 36 (2) (2011) 280.
[8] P.W. Metz, K. Hasse, D. Parisi, N.O. Hansen, C. Kränkel, M. Tonelli, G. Huber, Opt. Lett. 39 (17) (2014) 5158.
[9] P. Camy, J.L. Doualan, R. Moncorgé, J. Bengoechea, U. Weichmann, Opt. Lett. 32 (11) (2007) 1462.
[10] P.W. Metz, S. Muller, F. Reichert, D.T. Marzahl, F. Moglia, C. Krankel, G. Huber, Opt. Express 21 (25) (2014) 31274.
[11] A. Sottile, P.W. Metz, Opt. Lett. 40 (9) (2015) 1992.
[12] B. Xu, F. Starecki, D. Paboeuf, P. Camy, J.L. Doualan, Z.P. Cai, A. Braud, R. Moncorgé, Ph Goldner, F. Bretenaker, Opt. Express 21 (5) (2013) 5567.
[13] F. Reichert, F. Moglia, D.T. Marzahl, P. Metz, M. Fechner, N.O. Hansen, G. Huber, Opt. Express 20 (18) (2012) 20387.
[14] T.T. Basiev, V.A. Konyushkin, D.V. Konyushkin, M.E. Doroshenko, G. Huber, F. Reichert, N.O. Hansen, M. Fechner, Opt. Mater. Express 1 (8) (2011) 1511.
[15] A. Richter, H. Scheife, E. Heumann, G. Huber, W. Seelert, A. Diening, Electron. Lett. 41 (14) (2005) 794.
[16] Y. Fujitomo, M. Murakami, J. Nakanishi, T. Yamada, O. Ishii and M. Yamazaki, Advanced Solid-State Lasers Congress, Technical Digest OSA, paper AM2A.2., 2013.
[17] H. Okamoto, K. Kasuga, Y. Kubota, Opt. Lett. 36 (2011) 1470.
[18] H. Okamoto, K. Kasuga, I. Hara, Y. Kubota, Opt. Express 17 (2009) 20227.
[19] D.T. Marzahl, F. Reichert, P.W. Metz, M. Fechner, N.O. Hansen1, G. Huber, Appl. Phys. B 116 (1) (2014) 109.
[20] M. Fibrich, H. Jelínková, J. Šulc, K. Nejezchle, V. Škoda, Appl. Phys. B 97 (2009) 363.
[21] M. Malinovski, M.F. Joubert, B. Jacquier, Phys. Status Solidi (a) 140 (1993) K49.
[22] L.D. Merkle, B. Zandi, R. Moncorgé, Y. Guyot, H.R. Verdun, B. Mclntosh, J. Appl. Phys. 79 (4) (1996) 1849.
[23] J. Huang, S. Zhang, Y. Chen, X. Gong, Y. Lin, Z. Luo, Y. Huang, J. Am. Ceram. Soc. 96 (11) (2013) 3569.
[24] D.K. Sardar, C.C. Russell III, J. Appl. Phys. 95 (10) (2004) 5334 5339.
[25] L.D. Merkle, B. Zandi, Y. Guyot, H.R. Verdun, B. Mclntosh, B.H.T. Chai, J.B. Gruber, M.D. Seltzer, C.A. Morrison, R. Moncorgé, in: T.Y. Fan, B.H.T. Chai (Eds.), OSA Proceedings on Advanced Solid-State Lasers, Vol. 20, OSA, 1994, pp 361–366.
[26] A.O. Wright, M.D. Seltzer, J.B. Gruber, B. Zandi, L.D. Merkle, B.H.T. Chai, J. Phys. Chem. Solids 57 (9) (1996) 1337.
[27] J.Y. Allain, M. Monerie, H. Poignant, Electron. Lett. 27 (2) (1991) 189.
[28] B. Qu, R. Moncorgé, Z. Cai, J.L. Doualan, B. Xu, H. Xu, A. Braud, P. Camy, Opt. Lett. 40 (13) (2015) 3053.
[29] L.D. DeLoach, S.A. Payne, L.K. Smith, W.L. Kway, W.F. Krupke, J. Opt. Soc. Am. B 11 (2) (1994) 269.
[30] C. Morrison, Rep. Army Res. Lab. (1995) ARL-TR-708.
[31] S. Khiari, M. Velazquez, R. Moncorgé, J.L. Doualan, P. Camy, A. Ferrier, M. Diaf, J. Alloy. Compd. 451 (2008) 128.
[32] B.R. Judd, Phys. Rev. 127 (1962) 750.
[33] G.S. Ofelt, J. Chem. Phys. 37 (1962) 511.
[34] M.J. Weber, Phys. Rev. 157 (1967) 262.
[35] M.J. Weber, J. Chem. Phys. 48 (1968) 4774.
[36] Ph Goldner, F. Auzel, J. Appl. Phys. 79 (10) (1996) 7972.
[37] M.P. Hehlen, M.G. Brik, K.W. Krämer, J. Lumin. 136 (2013) 221.

Please cite this article as: B. Qu, et al., J. Lumin. (2016), http://dx.doi.org/10.1016/j.jlumin.2016.07.048

[38] A.A. Kornienko, A.A. Kaminskii, E.B. Dunina, Phys. Status Solidi (b) 157 (1990) 267.
[39] Z. Liu, B. Qu, J.L. Doualan, B. Xu, H. Xu, Z. Cai, A. Braud, P. Camy, R. Moncorgé, J. Opt. Soc. Am. B 32 (2) (2015) 263.
[40] V.M. Martins, G.A. Azevedo, A.A. Andrade, D.N. Messias, A.F.G. do Monte, N. O. Dantas, V. Pilla, T. Catunda, A. Braud, R. Moncorgé, Opt. Mater. 37 (2014) 387.
[41] D.I. Zalucha, J.C. Wright, F.K. Fong, J. Chem. Phys. 59 (1973) 997.
[42] J.C. Vial, R. Buisson, F. Madeore, M. Poirier, J. Phys. 40 (1979) 913.
[43] T.H. Allik, J.B. Gruber, M.D. Seltzer, M.E. Hills, K. Sparious, R.D. Stultz, M. Birnbaum, C.A. Morrison, B.H.T. Chai, J.A. Hutchinson, L.D. Merkle, in: A.A. Pinto, T.Y. Fan, (Eds). OSA Proceedings on Advanced Solid-State Lasers, Optical Society of America, Washington, DC, Vol. 15, 1993, pp. 246–249.

Please cite this article as: B. Qu, et al., J. Lumin. (2016), http://dx.doi.org/10.1016/j.jlumin.2016.07.048